Original Article

Novel biomarkers based on dual-energy computed tomography for risk stratification of very early distant metastasis in colorectal cancer after surgery

Wenjing Peng[1]^, Lijuan Wan[1], Rui Zhao[1], Shuang Chen[1], Shushan Dong[2], Lin Li[1], Hongmei Zhang[1]^

[1]Department of Radiology, National Cancer Center/National Clinical Research Center for Cancer/Cancer Hospital, Chinese Academy of Medical Sciences and Peking Union Medical College, Beijing, China; [2]Clinical Science, Philips Healthcare, Beijing, China

Contributions: (I) Conception and design: H Zhang, L Li; (II) Administrative support: H Zhang; (III) Provision of study materials or patients: W Peng, L Wan, R Zhao, S Chen; (IV) Collection and assembly of data: W Peng, L Wan, S Dong; (V) Data analysis and interpretation: W Peng, L Li, H Zhang; (VI) Manuscript writing: All authors; (VII) Final approval of manuscript: All authors.

Correspondence to: Lin Li, MD; Hongmei Zhang, MD. Department of Radiology, National Cancer Center/National Clinical Research Center for Cancer/Cancer Hospital, Chinese Academy of Medical Sciences and Peking Union Medical College, 17 Panjiayuan Nanli, Chaoyang District, Beijing 100021, China. Email: linlin77216@sina.com; 13581968865@163.com.

Background: Very early distant metastasis (VEDM) for patients with colorectal cancer (CRC) following surgery suggests failure of local treatment strategy and few biomarkers are available for its effective risk stratification. This study aimed to explore the potential of quantitative dual-energy computed tomography (DECT) spectral parameters and build models to predict VEDM.

Methods: Consecutive patients suspected of having CRC and with a clinical indication for enhanced CT from April 2021 to July 2022 at a single institution were prospectively enrolled to undertake spectral CT scanning. The spectral features were extracted by two reviewers and intraclass correlation coefficient (ICC) was used for interobserver agreement evaluation. A total of 16 spectral parameters, including unenhanced effective atomic number, triphasic iodine concentrations (ICs)/normalized ICs (NICs)-$_{A/V/E}$/1/NIC-$_{A/V/E}$/spectral curve slopes (λ-$_{A/V/E}$), two arterial enhancement fractions (AEFs), and venous enhancement fraction (VEF), were determined for analysis. Patients with and without VEDM after surgery were matched using propensity score matching (PSM). The diagnostic performance was assessed using the area under the curve (AUC). Models of multiple modalities were generated.

Results: In total, 222 patients were included (141 males, age range, 32–83 years) and 13 patients developed VEDM. Interobserver agreement ranged from good to excellent (ICC, 0.773–0.964). A total of three spectral parameters (VEF, λ-$_V$, and 1/NIC-$_V$) exhibited significant discriminatory ability ($P<0.05$) in predicting VEDM, with AUCs of 0.822 [95% confidence interval (CI): 0.667–0.926], 0.738 (95% CI: 0.573–0.866), and 0.713 (95% CI: 0.546–0.846) and optimal cutoff points of 67.16%, 2.46, and 2.44, respectively. The performance of these spectral parameters was validated in the entire cohort; the combined spectral model showed comparable efficiency to the combined clinical model [AUC, 0.771 (95% CI: 0.622–0.919) *vs.* 0.779 (95% CI: 0.663–0.894), $P>0.05$]; the clinical-spectral model achieved further improved AUC of 0.887 (95% CI: 0.812–0.962), which was significantly higher than the combined clinical model ($P=0.015$), yet not superior to the combined spectral model ($P=0.078$).

Conclusions: Novel spectral parameters showed potential in predicting VEDM in CRC following surgery in this preliminary study, which were closely related with spectral perfusion in the venous phase. However, further studies with larger samples are warranted.

^ ORCID: Wenjing Peng, 0000-0002-2771-1203; Hongmei Zhang, 0000-0002-2976-8414.

Keywords: Colorectal cancer (CRC); distant metastasis (DM); dual-energy computed tomography (DECT); propensity score

Submitted Jun 13, 2023. Accepted for publication Nov 29, 2023. Published online Jan 02, 2024.
doi: 10.21037/qims-23-861
View this article at: https://dx.doi.org/10.21037/qims-23-861

Introduction

Curative surgical resection is the preferred treatment for non-metastatic colon cancer and the standard treatment modality for locally advanced rectal cancer after neoadjuvant therapy (1,2). The crucial determinant of long-term prognosis following surgery is the occurrence of distant metastasis (DM). A proportion of patients with colorectal cancer (CRC) experience DM shortly after surgery in clinical practice. The earlier the metastasis occurs, the more challenging the treatment becomes and the worse the prognosis will be. DM as early as 6 months after surgery can be highly suggestive of aggressive biological behavior, and such patients can maximally benefit from the potentially adjusted treatment strategies. We define DM within 6 months after surgery as very early DM (VEDM). For these highly specific patients, blindly pursuing surgical treatment is likely to be aggressive, and a more systemic and comprehensive treatment strategy should be fully considered (3,4). Patients with locally advanced rectal cancer may also receive inappropriate local treatment strategies, leading to unnecessary radiation therapy harm. Preoperative risk stratification of VEDM is crucial for improving the prognosis of patients with CRC.

However, there is currently a lack of effective methods for early risk stratification of VEDM in patients with CRC following surgery. Extramural venous invasion (EMVI) serves as a relatively clear indicator of liver metastasis (5), the preoperative assessment of which relies on high-resolution magnetic resonance imaging (MRI) examinations. Nevertheless, the sensitivity and specificity reported has varied, and the consistency has been poor among reviewers (6,7). Moreover, for patients with colon cancer and those with rectal cancer who have contraindications for MRI, the efficacy of computed tomography (CT) in evaluating EMVI remains uncertain. CRC-associated tumor biomarkers, such as carcinoembryonic antigen (CEA) and carbohydrate antigen 19-9 (CA19-9), have also shown relatively low sensitivity and specificity in predicting DM (8,9). Therefore, it is highly necessary to find new and precise biomarkers for preoperatively predicting VEDM in patients with CRC after surgery.

CT is the preferred imaging method for colon cancer staging and is important for patients with rectal cancer who have MRI contraindications. Dual-energy CT (DECT) has rapidly developed in recent years, and a series of functional DECT parameters have shown potential in evaluating tumor heterogeneity, for example, the effective atomic number (Z-eff) (10-12), iodine concentration (IC) (13-15), and spectral curve slope (16). It is known that angiogenesis level or perfusion (17), and substance components are the key tumor microenvironment affecting metastasis and prognosis. Studies exploring the potential of DECT parameters in marking CRC for the risk stratification of VEDM are rare.

Our study aimed to explore the potential of the original or derived spectral parameters based on triphasic dynamic-enhanced DECT for quantitatively marking CRC and build models to predict VEDM for patients with CRC following surgery. We present this article in accordance with the TRIPOD reporting checklist (available at https://qims.amegroups.com/article/view/10.21037/qims-23-861/rc).

Methods

Patients

This study was conducted in accordance with the Declaration of Helsinki (as revised in 2013). The study protocol was approved by the Institutional Review Board of Chinese Academy of Medical Sciences and Peking Union Medical College (No. 2021-I2M-C&T-A-017), and written informed consent was provided by each patient before the CT examination.

Consecutive patients suspected of having CRC and with a clinical indication for enhanced CT from April 2021 to July 2022 at the Cancer Hospital, Chinese Academy of Medical Sciences and Peking Union Medical College were prospectively enrolled in this study. A total of 325 patients were included and undertook chest-abdomen-pelvis

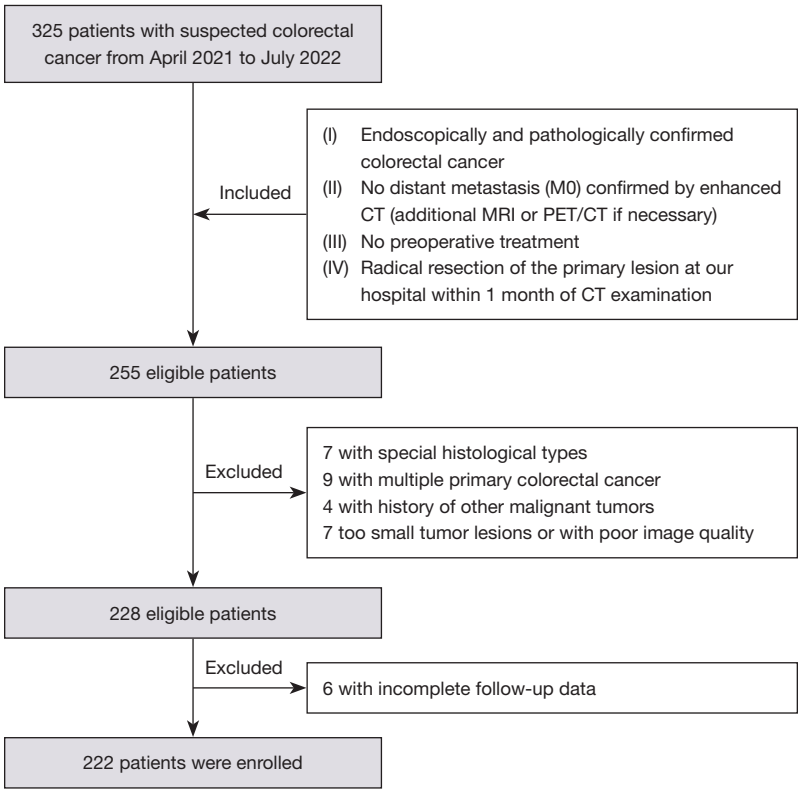

Figure 1 Flow chart showing patient inclusion. CT, computed tomography; MRI, magnetic resonance imaging; PET, positron emission tomography.

multiphasic dual-layer spectral detector CT (DLSCT) scanning, with abdominal CT including the unenhanced, arterial, venous, and equilibrium phases. Patients meeting the following criteria were included: (I) endoscopically and pathologically confirmed CRC; (II) no DM (M0) confirmed by enhanced CT [additional MRI or positron emission tomography (PET)/CT if necessary]; (III) no preoperative treatment; and (IV) underwent radical resection of the primary lesion at our hospital within 1 month of CT examination. A total of 27 patients were excluded for the following reasons: (I) special histological types, including mucinous adenocarcinoma, signet ring cell carcinoma, and medullary carcinoma (n=7); (II) multiple primary CRC (n=9); (III) history of other malignant tumors (n=4); and (IV) tumor lesions that were too small or had poor image quality for accurate delineation (n=7). Therefore, a total of 228 patients were included in the follow-up, consisting of evaluations at 1-month post-surgery, every 3 months thereafter, and with at least a 6-month follow-up period in total, according to the National Comprehensive Cancer Network (NCCN) guidelines. The occurrence of DM was recorded (including suspicious metastatic lesions obviously enlarged; lesions with typical metastatic imaging findings; metastatic lesions confirmed by pathological biopsy). A further 6 patients were excluded owing to incomplete follow-up data; 222 patients with CRC were included in the analysis. *Figure 1* illustrates the flowchart of participant inclusion.

Clinical information, including age, sex, and preoperative levels of CA19-9 and CEA was obtained from the hospital medical record system.

DECT scan

All CT scans were performed using a DLSCT scanner (iQon Spectral CT, Philips Healthcare, Best, the Netherlands). Patients were asked to fast overnight and undergo bowel preparation with polyethylene glycol prior to examination. Before scanning, 10 mL of raceanisodamine hydrochloride was injected intramuscularly (except in patients with contraindications), and the intestinal tract was inflated with gas to achieve distension. Subsequently, a routine

unenhanced scan was performed, followed by contrast-enhanced scans following intravenous administration of iodinated contrast media (80–90 mL of iodixanol, 320 mgI/mL; Hengrui Medicine, Lianyungang, China), at a rate of 3.0 mL/s. A bolus tracking technique was employed to determine the timing of the dynamic scan, with the descending aorta used as the target vessel. Dynamic-enhanced scanning was triggered 10 seconds after the CT value reached 150 Hounsfield units (HU). The arterial phase was obtained approximately 35 seconds after the start of the contrast agent injection, followed by the venous phase 25 seconds after the arterial phase; the equilibrium phase was 90 seconds after the venous phase. Arterial phase scanning covered the area from the lung apex to the lower margin of the symphysis pubis, whereas unenhanced, venous, and equilibrium phase scans covered the area from the diaphragmatic dome to the lower margin of the symphysis pubis. After scanning, conventional images were obtained using hybrid iterative reconstruction, and spectral-based images (SBIs) were generated using projection space spectral reconstruction. The reconstruction layer thickness and interval for both methods were 1.0 mm. The imaging acquisition parameters were set as follows: collimator width, 64 mm × 0.625 mm; rotation time, 0.28 seconds; tube voltage, 120 kVp; spectral CT adaptive current (range, 78–145 mAs); tube rotation speed, 0.5 s/r; pitch, 0.969.

DECT spectral feature extraction

The regions of interest (ROIs) were delineated and the DECT spectral features were extracted by two radiologists with 4 and 6 years of experience in abdominal imaging who were unaware of the clinical or histological information for each patient. Prior to formal delineation, focused training was conducted on 20 patients. Cases with significant differences in ROI delineation were reviewed by consensus, and a unified delineation standard and parameter extraction process were agreed upon. The specific steps were as follows: First, all the SBI data were transferred to the Philips IntelliSpace Portal spectral workstation (version 9), and access to the "Spectral Analysis" mode was obtained. Then, on 70 keV virtual mono-energetic images in the venous phase, a circular or elliptical ROI was placed on the slice with the maximum tumor, avoiding obvious calcifications, hemorrhages, necrotic cavities, and artifacts within the lesion. In the same lesion slice, a circular ROI was placed within the abdominal aorta or iliac artery lumen (avoiding vessel wall calcification and confirming that the ROI area covered at least 50% of the arterial cross-section). Finally, the corresponding ROIs were propagated to the same anatomical slice of different phases, and the spectral features were extracted by switching to different spectral windows.

The sum of parameters, including unenhanced Z-eff, triphasic ICs, and triphasic attenuations on the 40- and 80-keV virtual mono-energetic images for CRC were extracted (*Figure 2*). The mean of the measurements from two radiologists was regarded as the final measurement. The same-slice artery was used to normalize the ICs of CRC, reducing the impact of individual hemodynamic differences: normalized IC (NIC) = IC_{lesion}/IC_{artery}. Then, multiple derived parameters were calculated as follows: (I) spectral curve slope (λ) = $(CT_{40\ keV} - CT_{80\ keV})/40$; (II) triphasic enhancement fractions: arterial enhancement fraction (AEF) was defined as the ratio of $NIC_{arterial}$ to NIC_{venous} (×100%), as previously described (18,19), which we denoted as AEF1; AEF2 was defined as the ratio of $NIC_{arterial}$ to $NIC_{equilibrium}$ (×100%). We also defined venous enhancement fraction (VEF) as the ratio of NIC_{venous} to $NIC_{equilibrium}$ (×100%). Using prototypic software, we created quantitative color maps for the enhancement fractions, which allowed the triphasic datasets to be precisely aligned in three dimensions to correct the mismatches attributed to breathing. The resulting data of the enhancement fractions were mapped to a color scale displayed from purple to red (0–100%), then fused with the virtual plain scan images in the venous phase for more anatomic landmarks; and (III) 1/NIC = $1/NIC_{lesion}$. We assumed that the reciprocal perfusion parameters may in another dimension reflect the hemodynamic characteristics in tumors.

In summary, 16 DECT spectral parameters, in original or derived, were obtained for the subsequent analyses, namely unenhanced Z-eff, $IC\text{-}_A$, $IC\text{-}_V$, $IC\text{-}_E$, $NIC\text{-}_A$, $NIC\text{-}_V$, $NIC\text{-}_E$, $\lambda\text{-}_A$, $\lambda\text{-}_V$, $\lambda\text{-}_E$, AEF1, AEF2, VEF, $1/NIC\text{-}_A$, $1/NIC\text{-}_V$, and $1/NIC\text{-}_E$.

Evaluation of CT morphological features

All CT morphological features were evaluated using multiplanar reconstructed images with a slice thickness of 1 mm. The same two radiologists independently conducted the evaluation 4 weeks post-extraction of spectral parameters and were blinded to the patient's clinical or histopathological information. Prior to formal evaluation, the radiologists were trained by a senior radiologist with 22 years of experience and achieved a unified evaluation

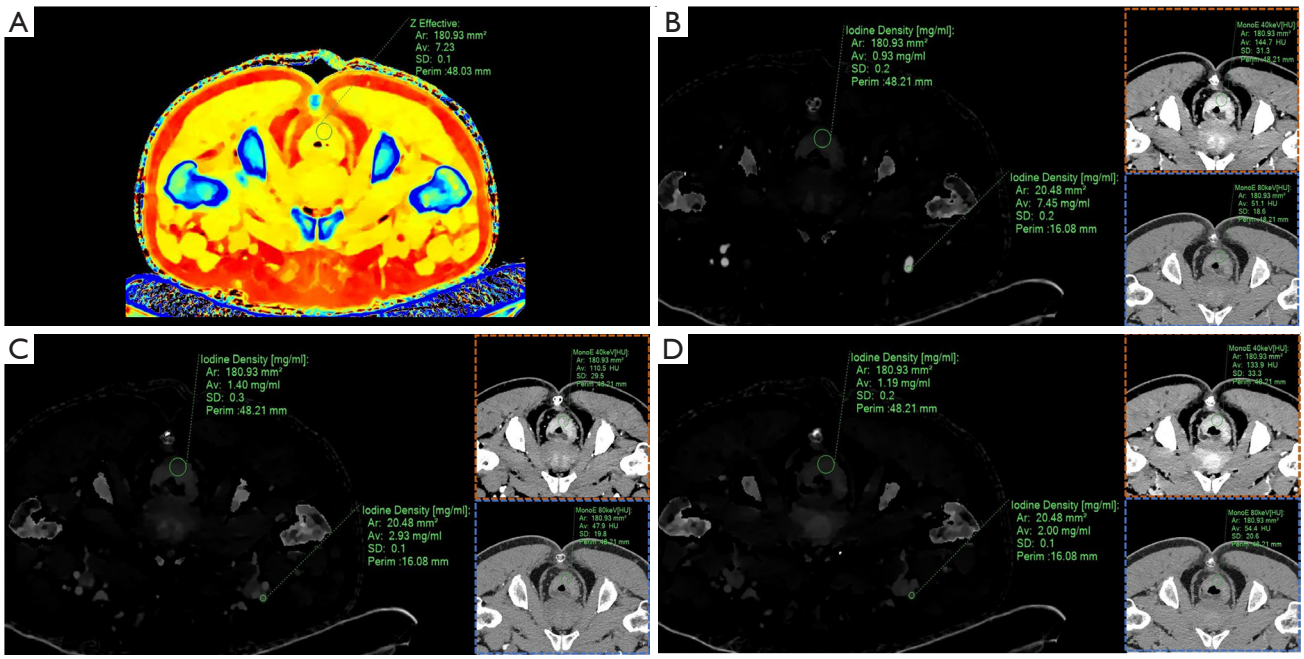

Figure 2 Delineation of ROIs and spectral measurement extraction on images of a 61-year-old male with pathologically confirmed rectal cancer. (A) Effective atomic number for the lesion on the unenhanced image: 7.23. (B-D) Triphasic ICs for the lesion and artery (the left part of each image), as well as triphasic attenuations for the lesion on the 40- and 80-KeV virtual mono-energetic images (the right part of each image). (B) The arterial phase, IC_{lesion}: 0.93 mg/mL; IC_{artery}: 7.45 mg/mL; $CT_{40\ keV}$: 144.7 HU; $CT_{80\ keV}$: 51.1 HU. (C) The venous phase, IC_{lesion}: 1.40 mg/mL; IC_{artery}: 2.93 mg/mL; $CT_{40\ keV}$: 110.5 HU; $CT_{80\ keV}$: 47.9 HU. (D) The equilibrium phase, IC_{lesion}: 1.19 mg/mL; IC_{artery}: 2.00 mg/mL; $CT_{40\ keV}$: 133.9 HU; $CT_{80\ keV}$: 54.4 HU. Ar, area; Av, average; SD, standard deviation; Perim, perimeter; MonoE, mono-energy; ROI, region of interest; ICs, iodine concentrations; CT, computed tomography; HU, Hounsfield unit.

standard. The consensus was achieved after a joint review in cases of discrepancies in qualitative parameters, and means of quantitative morphological parameters were used for subsequent statistical analyses. CT morphological features including tumor location, CT-based T stage (ctT) (20), N stage (ctN) (21), EMVI (ctEMVI) (5), maximum tumor circumferential percentage (MCP), maximum tumor length (MTL), and maximum tumor thickness (MTT) were recorded. Table S1 lists the standards used for evaluating these features.

Statistical analysis

Interobserver agreement for the DECT spectral parameters was evaluated using the intraclass correlation coefficient (ICC) with a 95% confidence interval (CI). A correlation was regarded as excellent, good, moderate, fair, and poor, if the ICC value was >0.8, ≤0.8 to >0.6, ≤0.6 to >0.4, ≤0.4 to >0.2, and ≤0.2, respectively.

Owing to the low incidence of VEDM in the study participants and the trend of inadequate adjustment of confounding covariates in the multivariable regression analysis, we adopted a more flexible and robust alternative analysis method, propensity score matching (PSM). Patients with metastases were matched to those without metastases using PSM. A propensity score (logit model) was calculated for all patients based on baseline clinical and CT morphological characteristics, including age, sex, location, CA19-9, CEA, ctT, ctN, ctEMVI, MCP, MTL, and MTT (excluding patients with missing values). A 1:2 matching protocol was performed to select the matched non-metastatic group with no replacement (optimal-matching algorithm). The clinical and CT characteristics were compared before and after PSM between the metastatic and non-metastatic groups. Continuous variables were compared by using the Student's *t*-test or Mann-Whitney *U* test according to the Q-Q plot. Categorical data were analyzed using the chi-square test or Fisher's exact test. In the cohort after PSM, spectral features were compared similarly between the metastatic and non-metastatic groups.

They were analyzed via univariable regression analysis to investigate the discriminatory significance. The optimal cutoff points were identified using receiver operating characteristic (ROC) curves, at which the maximum Youden indices were achieved.

The entire cohort before PSM was used to validate the performance of the spectral parameters. All significant spectral features in the entire cohort were transformed into binary variables using optimal cutoff values and reassessed via univariable regression analysis. The combined spectral model was established using multivariable regression analysis (method: enter). The combined clinical model was afterward constructed by entering all the significant baseline clinical and CT morphological characteristics in univariable analysis. Similarly, a clinical-spectral model integrating all significant clinical and spectral parameters in the univariable analysis was established. The area under the curve (AUC) was employed for evaluating the efficiency of the models. The models were compared using the DeLong test. Decision curve analysis (DCA) was used to test the clinical usefulness of models. Analyses were performed using SPSS version 25.0 (IBM Corp., Armonk, NY, USA), R version 3.4.1 (The R Foundation for Statistical Computing, Vienna, Austria), and MedCalc version 20.010 (MedCalc Software, Ostend, Belgium). A two-tailed P value <0.05 was considered statistically significant.

Results

Patient characteristics

In total, 222 patients were included in the study (mean age ± standard deviation, 59±10 years; age range, 32–83 years; 141 males). A total of 13 patients developed VEDM within a 6-month follow-up, accounting for a rate of 5.9%, of which 9 presented with single liver metastasis, 1 with single lung metastasis, 1 with solitary peritoneal metastasis, 1 with both lung and liver metastases, and 1 with retroperitoneal lymph node and liver metastases. The clinical and CT morphological features of metastatic and non-metastatic groups before and after PSM are listed in *Table 1*, and the distribution of the propensity scores is shown in *Figure 3*. After PSM, 13 metastatic and 26 non-metastatic patients were included in the analysis. Before matching, ctEMVI was significantly different between metastatic and non-metastatic groups (P=0.001), whereas after matching, all baseline clinical and CT morphological parameters were balanced (all P>0.05).

Interobserver agreement for DECT spectral parameters

Interobserver agreement for the DECT spectral parameters was good to excellent, with ICC ranging from 0.773 (95% CI: 0.714–0.821) to 0.964 (95% CI: 0.952–0.973). Details of the interobserver agreement are provided in *Table 2*.

Apparent performance of DECT spectral parameters

In the cohort after PSM, all 16 DECT spectral parameters were analyzed by univariable regression analysis to identify significant predictors and only VEF, λ-$_V$, and 1/NIC-$_V$ exhibited significant discriminatory ability between the metastatic and non-metastatic groups (Table S2). The box plots and ROC curves of the three discriminatory spectral parameters are shown in *Figure 4*. The other parameters, including unenhanced Z-eff, triphasic ICs, triphasic NICs, AEF1, AEF2, λ-$_A$, λ-$_E$, 1/NIC-$_A$, and 1/NIC-$_E$) showed no significant findings (P>0.05).

The VEF values of metastatic patients (median: 0.638; range, 0.461–0.852) were significantly lower than those of non-metastatic patients (median: 0.774; range, 0.465–1.040; *Figure 4A*; P=0.002), which achieved an AUC of 0.822 (95% CI: 0.667–0.926), a sensitivity of 76.92%, and a specificity of 80.77% at a cutoff value of 67.16% (*Figure 4D*). On the VEF color maps, patients with metastases were indicated in red or orange, whereas those without metastases were indicated in yellow and green (*Figure 5*).

The λ-$_V$ values of metastatic patients (median: 2.063; range, 0.863–3.300) were significantly lower than those of non-metastatic patients (median: 2.838; range, 1.450–3.625; *Figure 4B*; P=0.008). The predicted AUC was 0.738 (95% CI: 0.573–0.866), with a sensitivity of 76.92% and a specificity of 73.08% at a cutoff value of 2.46 (*Figure 4E*).

The 1/NIC-$_V$ values of metastatic patients (median: 2.679; range, 1.484–4.650) were significantly higher than those of non-metastatic patients (median: 2.156; range, 1.628–2.913; *Figure 4C*; P=0.043). The predicting AUC was 0.713 (95% CI: 0.546–0.846), with a sensitivity of 69.23% and a specificity of 80.77% at a cutoff value of 2.44 (*Figure 4F*).

VEF exhibited the highest predictive power among the parameters; the difference between the three parameters was not statistically significant (P>0.05).

Validation of the performance of DECT spectral parameters in the entire cohort

The validated performance of each single and combined

Table 1 The clinical and CT morphological characteristics of patients with and without VEDM before and after propensity score matching

Characteristics	Before matching			After matching		
	Non-VEDM (n=209)	VEDM (n=13)	P value	Non-VEDM (n=26)	VEDM (n=13)	P value
Age (years)	61 [53–67]	55 [54–66]	0.395	58 [53–65]	55 [54–66]	0.918
Sex			0.054			>0.99
Female	80 (38.3)	1 (7.7)		2 (7.7)	1 (7.7)	
Male	129 (61.7)	12 (92.3)		24 (92.3)	12 (92.3)	
Tumor location			0.391			>0.99
Rectum	120 (57.4)	8 (61.5)		16 (61.5)	8 (61.5)	
Sigmoid colon	42 (20.1)	5 (38.5)		10 (38.5)	5 (38.5)	
Transverse colon	6 (2.9)	0 (0.0)		0 (0.0)	0 (0.0)	
Cecum and right colon	30 (14.4)	0 (0.0)		0 (0.0)	0 (0.0)	
Left colon	11 (5.3)	0 (0.0)		0 (0.0)	0 (0.0)	
CA19-9			0.732			0.643
≤30 U/mL	176 (84.2)	12 (92.3)		21 (80.8)	12 (92.3)	
>30 U/mL	31 (14.8)	1 (7.7)		5 (19.2)	1 (7.7)	
NA	2 (1.0)	0 (0.0)		0 (0.0)	0 (0.0)	
CEA			0.068			>0.99
≤5 ng/mL	143 (68.4)	5 (38.5)		10 (38.5)	5 (38.5)	
>5 ng/mL	63 (30.1)	8 (61.5)		16 (61.5)	8 (61.5)	
NA	3 (1.4)	0 (0.0)		0 (0.0)	0 (0.0)	
ctT			0.279			>0.99
1	12 (5.7)	0 (0.0)		0 (0.0)	0 (0.0)	
2	39 (18.7)	0 (0.0)		0 (0.0)	0 (0.0)	
3	71 (34.0)	6 (46.2)		13 (50.0)	6 (46.2)	
4	87 (41.6)	7 (53.8)		13 (50.0)	7 (53.8)	
ctN			0.280			>0.99
Negative	136 (65.1)	6 (46.2)		12 (46.2)	6 (46.2)	
Positive	73 (34.9)	7 (53.8)		14 (53.8)	7 (53.8)	
ctEMVI			0.001*			0.689
Negative	132 (63.2)	2 (15.4)		7 (26.9)	2 (15.4)	
Positive	77 (36.8)	11 (84.6)		19 (73.1)	11 (84.6)	
MCP			0.521			>0.99
1	39 (18.7)	1 (7.7)		2 (7.7)	1 (7.7)	
2	41 (19.6)	4 (30.8)		7 (26.9)	4 (30.8)	
3	37 (17.7)	1 (7.7)		2 (7.7)	1 (7.7)	
4	92 (44.0)	7 (53.8)		15 (57.7)	7 (53.8)	

Table 1 (*continued*)

Table 1 (*continued*)

Characteristics	Before matching			After matching		
	Non-VEDM (n=209)	VEDM (n=13)	P value	Non-VEDM (n=26)	VEDM (n=13)	P value
MTL (cm)	4.2 [2.9–5.4]	4.7 [3.3–6.1]	0.254	4.5 [3.9–5.7]	4.7 [3.3–6.1]	0.706
MTT (cm)	1.5 [1.2–1.9]	1.7 [1.4–2.4]	0.092	1.9 [1.4–2.2]	1.7 [1.4–2.4]	0.706

Data are presented as median [IQR] or n (%). *, statistical significance. CT, computed tomography; VEDM, very early distant metastasis; CA19-9, carbohydrate antigen 19-9; NA, not available; CEA, carcinoembryonic antigen; ctT, CT-based T stage; ctN, CT-based N stage; ctEMVI, CT-based EMVI; EMVI, extramural vascular invasion; MCP, maximum tumor circumferential percentage; MTL, maximum tumor length; MTT, maximum tumor thickness.

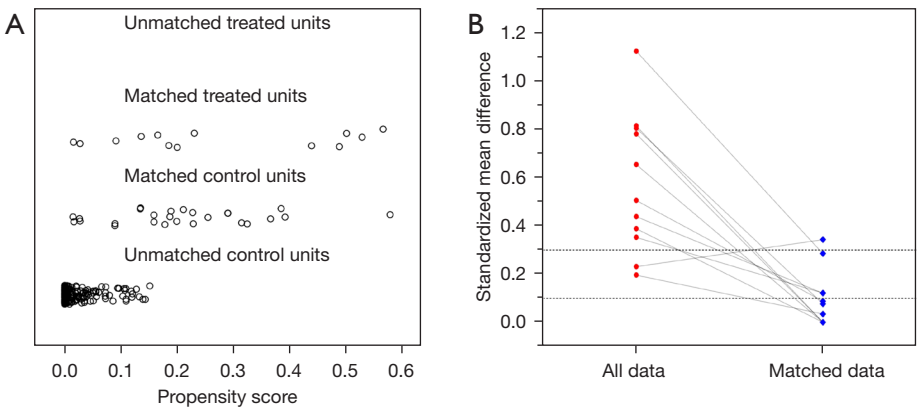

Figure 3 Propensity scores of the baseline clinical and CT morphological characteristics before and after matching. (A) Dot plot showing the distribution of propensity scores in both matched and unmatched cohorts. (B) Line plot showing the standardized mean differences before and after matching. The two dashed lines represent standardized mean difference values of 0.1 and 0.3, respectively. CT, computed tomography.

Table 2 Interobserver agreement for the spectral parameters

Phases	Variables	ICC (95% CI)
Unenhanced	Lesion Z-eff	0.816 (0.767–8.856)
Arterial phase	Lesion IC	0.859 (0.820–0.890)
	Artery IC	0.964 (0.952–0.973)
	Lesion $CT_{40\ keV}$	0.860 (0.821–0.891)
	Lesion $CT_{80\ keV}$	0.825 (0.771–0.866)
Venous phase	Lesion IC	0.898 (0.868–0.921)
	Artery IC	0.952 (0.937–0.963)
	Lesion $CT_{40\ keV}$	0.903 (0.874–0.925)
	Lesion $CT_{80\ keV}$	0.844 (0.794–0.881)
Equilibrium phase	Lesion IC	0.865 (0.827–0.895)
	Artery IC	0.91 (0.885–0.931)
	Lesion $CT_{40\ keV}$	0.857 (0.817–0.888)
	Lesion $CT_{80\ keV}$	0.773 (0.714–0.821)

ICC, intraclass correlation coefficient; CI, confidence interval; IC, iodine concentration; CT, computed tomography.

predictors in the entire cohort before PSM is shown in *Figure 6*. VEF, λ-$_V$, and 1/NIC-$_V$ of all patients were first subjected to binary classification conversion according to the aforementioned cut-off values. VEF (P=0.001) and λ-$_V$ (P=0.016) remained significant in predicting VEDM, whereas 1/NIC-$_V$ was not (P=0.107). The AUCs of VEF, λ-$_V$, and 1/NIC-$_V$ for predicting VEDM were 0.730 (95% CI: 0.580–0.879), 0.679 (95% CI: 0.529–0.829), and 0.618 (95% CI: 0.466–0.770), respectively (*Figure 6A*). The VEF yielded the highest predictive utility among the three parameters; however, the difference was not statistically significant (P>0.05). The combined spectral model enrolling the three parameters showed a higher AUC of 0.771 (95% CI: 0.622–0.919) (*Figure 6B*).

Comparisons between different models

In the entire cohort before PSM, two clinical and CT morphological parameters, CEA and ctEMVI, were

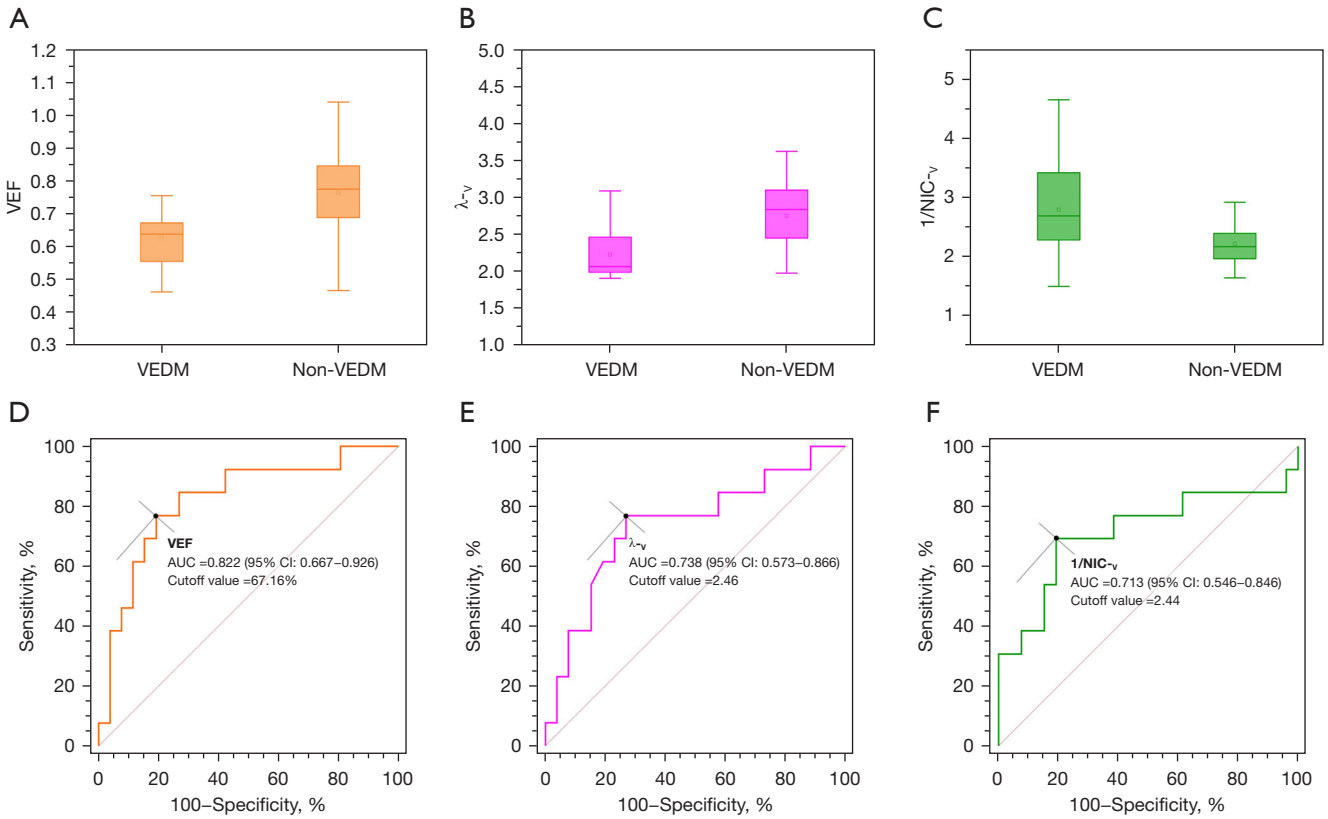

Figure 4 Box plots and ROC curves of discriminatory spectral parameters for VEDM in PSM cohort. (A-C) Box plots showing VEF, λ-$_V$, and 1/NIC-$_V$ between patients with and without VEDM in the PSM cohort. (D-F) ROC curves of VEF, λ-$_V$, and 1/NIC-$_V$ in predicting VEDM, which identifies the optimal cutoff points. VEF, venous enhancement fraction; VEDM, very early distant metastasis; NIC, normalized iodine concentration; AUC, area under the curve; CI, confidence interval; ROC, receiver operating characteristic; PSM, propensity score matching.

significantly predictive of VEDM (P=0.029 and P=0.004, respectively; Table S2). The predictive AUC values for CEA and ctEMVI were 0.655 (95% CI: 0.497–0.813) and 0.736 (95% CI: 0.611–0.861), respectively (*Figure 6A*). The combined clinical model showed a higher AUC of 0.779 (95% CI: 0.663–0.894), whereas that of the clinical-spectral model combining the clinical and spectral parameters was 0.887 (95% CI: 0.812–0.962) (*Figure 6B*). The clinical-spectral model achieved a sensitivity of 92.31% and a specificity of 72.82%, respectively. Parameters, as well as their coefficients and model intercept retained in the clinical-spectral model are presented in *Table 3*.

The clinical-spectral model achieved the highest AUC in predicting VEDM and was superior to each spectral and clinical predictor (all P<0.05). The clinical-spectral model showed a significantly higher performance than the combined clinical model (AUC, 0.887 *vs.* 0.779, P=0.015); however, it was not statistically superior to the combined spectral model (AUC, 0.887 *vs.* 0.771, P=0.078). The performance of the combined spectral model was comparable to that of the combined clinical model (AUC, 0.771 *vs.* 0.779, P>0.05), and every single spectral parameter showed similar performance to the single clinical parameter (all P>0.05). *Table 4* lists the apparent performance of each single and combined spectral, clinical, and clinical-spectral models in the entire cohort, as well as comparisons between models. Further comparisons using DCA also confirmed the added clinical application value of spectral parameters in predicting VEDM (*Figure 6C*).

Discussion

Our study, as a preliminary exploration, revealed the predictive potential of the (newly) derived quantitative

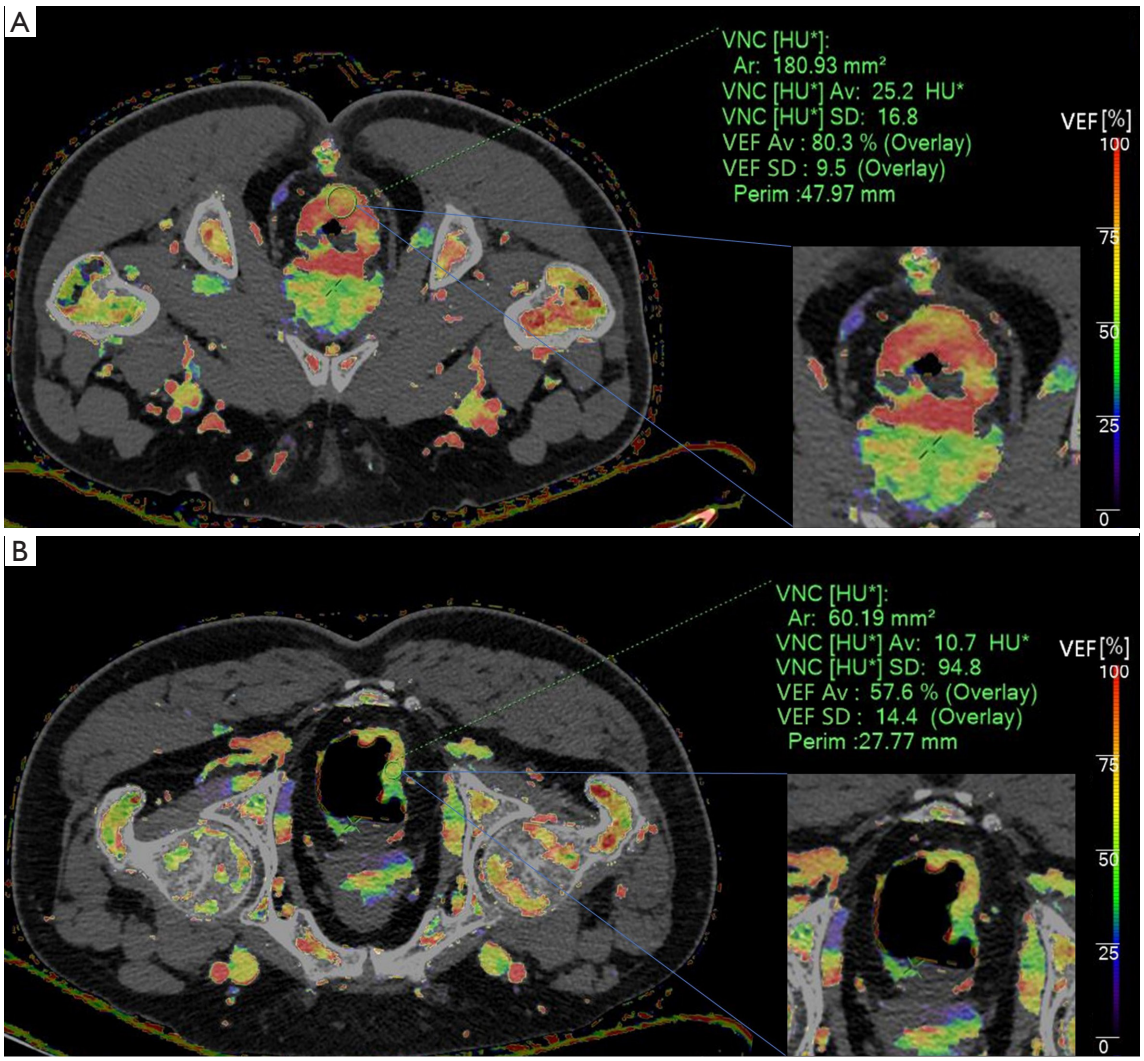

Figure 5 Comparison of VEF color maps between patients with and without VEDM post-surgery. (A) VEF color map of a 61-year-old male with surgery confirmed rectal cancer (T3N1c, EMVI+). The VEF value was high at 80.3%; a large portion of the tumor is indicated in red or orange. The patient developed a solitary liver metastasis 3 months following surgery. (B) VEF color map of another 61-year-old male with surgery confirmed rectal cancer (T3N1b, EMVI+). The VEF value was low at 57.6%; a large portion of the tumor is indicated in mixed yellow and green. No evidence of DM was observed within the 6-month follow-up. VNC, virtual plain scan; HU, Hounsfield unit; Ar, area; Av, average; SD, standard deviation; Perim, perimeter; VEF, venous enhancement fraction; VEDM, very early distant metastasis; EMVI, extramural vascular invasion; DM, distant metastasis.

DECT spectral parameters, including VEF, λ-$_V$, and 1/NIC-$_V$, for VEDM in CRC following surgery. Conventional IC/NIC measurements in three phases, as well as parameters of unenhanced Z-eff, AEF1, AEF2, λ-$_A$, λ-$_E$, 1/NIC-$_A$, and 1/NIC-$_E$ demonstrated no significant predictive efficiency. The performance of the three spectral predictors was validated in the entire cohort before PSM, which, in combination, showed comparable utility to that of the combined clinical model (AUC, 0.771 *vs.* 0.779, P>0.05). The DECT spectral parameters significantly improved the efficiency of the traditional clinical predictors (AUC, 0.887 *vs.* 0.779, P<0.05), and the clinical-spectral model yielded the highest predicting utility.

Tumor angiogenesis plays a critical role in facilitating metastasis (17). Traditionally, perfusion CT has been the preferred method to track the uptake of iodinated contrast

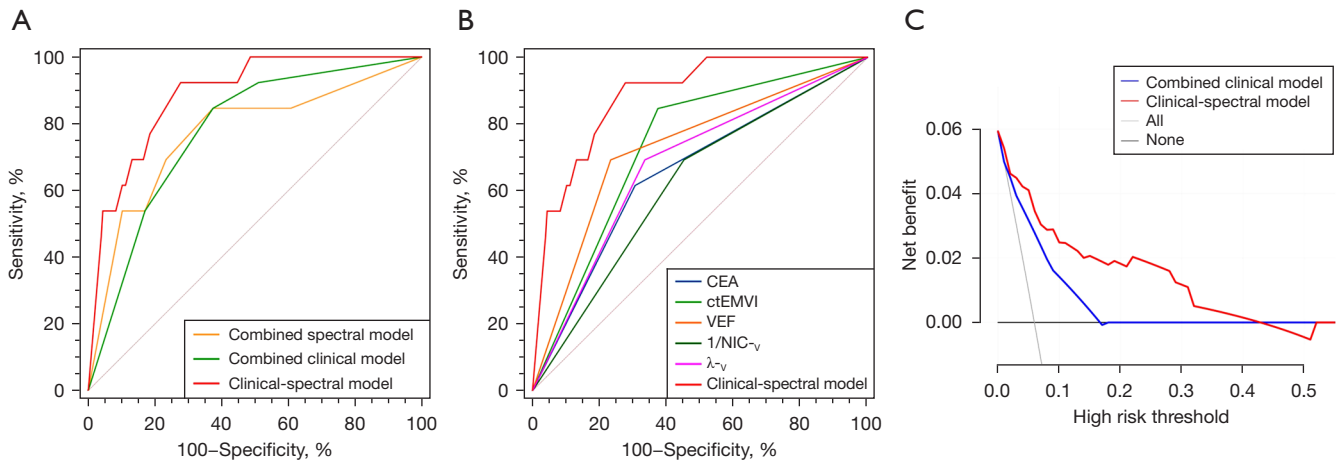

Figure 6 Apparent performance of each single and combined spectral, clinical, and clinical-spectral model in the entire cohort, as well as clinical utility evaluation using DCA. (A) ROC curves validating the performance of each discriminatory spectral parameter in predicting VEDM in the entire cohort (AUC: VEF, 0.730; λ-$_V$, 0.679; 1/NIC-$_V$, 0.618), as well as ROC curves of single clinical predictor (AUC: CEA, 0.655; ctEMVI, 0.736). Each spectral and clinical predictor exhibited moderate utility in predicting VEDM, inferior to the clinical-spectral model. (B) ROC curves showing the performance of the combined clinical, spectral, and clinical-spectral models (AUC, 0.779, 0.771, and 0.887, respectively). (C) DCA curves confirming the added clinical application value of the spectral parameters. The slash curve (All) indicates that all patients developed VEDM. The horizontal line (None) indicates that no patients developed VEDM. The two curves (clinical-spectral and combined clinical models) represent the clinical application value for the prediction of VEDM. When the threshold probability was 0–0.42, the net benefit of using the clinical-spectral model to predict VEDM was greater than that of using the single clinical model. CEA, carcinoembryonic antigen; ctEMVI, CT-based EMVI; EMVI, extramural vascular invasion; VEF, venous enhancement fraction; NIC, normalized iodine concentration; DCA, decision curve analysis; ROC, receiver operating characteristic; VEDM, very early distant metastasis; AUC, area under the curve.

Table 3 Parameters retained in the clinical-spectral model for predicting VEDM

Variables	β	OR
VEF	1.928	6.877
λ-$_V$	1.378	3.969
1/NIC-$_V$	–0.413	0.661
CEA	0.855	2.352
ctEMVI	2.287	9.847
Intercept	–5.977	–

VEDM, very early distant metastasis; OR, odds ratio; VEF, venous enhancement fraction; NIC, normalized iodine concentration; CEA, carcinoembryonic antigen; ctEMVI, CT-based EMVI; EMVI, extramural vascular invasion.

agents and measure angiogenesis (13-15); however, it delivers a high radiation dose and a large variance in perfusion parameters exists in different scanning techniques. Quantitative IC maps recently has shown great potential in replacing perfusion CT (13-15), which could further characterize tumor aggression.

Specifically in this study, the smaller values of VEF and λ-$_V$, along with larger values of 1/NIC-$_V$, were associated with a higher likelihood of VEDM occurrence. VEF reflects the ratio of perfusion in the venous phase to that of the equilibrium phase, and it can be smaller when CRC exhibits reduced venous input or increased equilibrium input. Additionally, 1/NIC-$_V$ demonstrates an inverse proportional and nonlinear relationship between perfusion in the venous phase. The smaller the NIC-$_V$, the larger the 1/NIC-$_V$ value. The parameter λ-$_V$ also involves perfusion characteristics regarding the venous phase. Consequently, all the significant parameters were closely related to spectral perfusion in the venous phase. It is known that tumor cells initiate colonization within organs through a series of intricate processes prior to DM (22). This localization in the microvascular region makes it susceptible to the formation of tumor thrombi owning to the tumor cell accumulation or polymerization with platelets and white blood cells (23).

Table 4 Apparent performance of each single and combined spectral, clinical, and clinical-spectral model in the entire cohort for predicting VEDM, and comparisons between models

Models	Predictors	AUC (95% CI)	P value
Spectral models	VEF	0.730 (0.580–0.879)	0.016*
	λ-$_V$	0.679 (0.529–0.829)	<0.001*
	1/NIC-$_V$	0.618 (0.466–0.770)	<0.001*
	Combination of VEF, λ-$_V$, and 1/NIC-$_V$	0.771 (0.622–0.919)	0.078
Clinical models	CEA	0.655 (0.497–0.813)	0.002*
	ctEMVI	0.736 (0.611–0.861)	<0.001*
	Combination of CEA and ctEMVI	0.779 (0.663–0.894)	0.015*
Clinical-spectral model	All the clinical and spectral predictors	0.887 (0.812–0.962)	Reference

*, statistical significance. VEDM, very early distant metastasis; AUC, area under the curve; CI, confidence interval; VEF, venous enhancement fraction; NIC, normalized iodine concentration; CEA, carcinoembryonic antigen; ctEMVI, CT-based EMVI; EMVI, extramural vascular invasion.

Given that the liver is the most frequently affected organ in VEDM in this study, we hypothesized that the presence of early liver microcirculation thrombi in patients with VEDM could elevate portal vein pressure, subsequently reducing blood supply in the venous phase for CRC. Limited by our preliminary study, further verification is warranted through foundational research in the future. Furthermore, aggressive behavior such as VEDM may indicate greater vascular permeability or tumor stromal volume of the primary lesion. The greater tumor vascular permeability allows tumor cells to pass through the gaps between endothelial cells or damaged basement membranes, thus participating in DM. The elevated tumor stromal volume or proportion is associated with poor prognosis (24,25). Both of the two indicators can manifest as increased input in the equilibrium phase (26) and result in a decreased VEF. Varying from the previous study (27), AEF1 did not show predictive efficiency for VEDM, which was possibly attributed to varying hemodynamic characteristics among tumors. In addition, the decreased perfusion in the venous phase can account for the correlation observed between 1/NIC-$_V$ and VEDM. Consistent with previous studies, the spectral curve slope demonstrated good predictive value for tumor invasiveness (12,28).

Contrary to the majority of prior studies, which successfully established correlation between pure IC/NIC measurements in primary lesions and tumor aggressiveness, neither the triphasic IC nor the triphasic NIC measurements demonstrated significant predictive power for VEDM in this study. We postulated that the previous studies had primarily focused on evaluating the invasion potential of the primary tumor site itself, including factors such as differentiation and peritumoral invasion (29-31). The involved hemodynamic variations were relatively straightforward. In contrast, this study was aimed at predicting metachronous metastasis in distant sites, which potentially entails more intricate spatio-temporal changes in hemodynamics. Therefore, the limited effectiveness of the pure IC/NIC measurements in this context was understandable.

In clinical practice, a single preoperative feature for predicting CRC metastasis is insufficient, and consensus on the best subset of predictors remains lacking, while EMVI and CEA are the fixed ones. Consistent with the previous results, both ctEMVI and CEA showed moderate efficiency in predicting metastasis, and the combined clinical model yielded an AUC of 0.779. Comparison between the combined clinical and spectral models showed no statistical difference. However, the performance of the clinical model was significantly improved following integration with the DECT spectral parameters, confirming the added value of the spectral parameters in predicting VEDM. The clinical-spectral model exhibited the highest efficiency and clinical usefulness. Hence, these models can potentially help clinicians to stratify the risk of VEDM in patients with CRC after surgery, instruct more proactive preoperative screening, more personalized perioperative treatment, and intensive adjustment for postoperative surveillance to improve long-term prognosis.

In this study, we used PSM to analyze the DECT spectral

parameters. Previous studies have indicated that spectral parameter values may be influenced by morphological and clinical features. For example, the size of the tumor may affect the IC value; the larger the tumor, the smaller the IC value (26,32). EMVI can also affect the clearance of iodine contrast agents in the equilibrium phase, resulting in a passive increase in IC value (30). The multivariable logistic regression model may not adjust for the confounding factors adequately, considering the low morbidity of VEDM in the real world and this study. Therefore, we used PSM to balance the potential confounding effects of baseline clinical and CT features to obtain more accurate results regarding spectral variables. Our validation results demonstrated the robustness of the PSM analysis.

There are some limitations in our study. First, it was a small positive-sample-sized study in a single center. In actuality, the overall cohort size was substantial (222 patients) in this prospective study, and patients with VEDM were identified as having undergone a rigorous and standardized follow-up strategy. These approaches may allow us to closely mirror the incidence of VEDM with real-world rates. In addition, to minimize the potential biases in data analysis, we applied PSM analysis to reduce confounding factors and also conducted a secondary validation across the entire cohort. Despite this, we provided a preliminary insight into potential spectral predictor for VEDM, and further verification is warranted through studies with larger sample sizes in the future. Second, this study only included images from a DLSCT scanner, which may limit the generalizability of the results to other DECT applications. The use of a single scanner can eliminate the bias in parameter acquisition caused by inter-scanner variability, making the conclusions more reliable. Moreover, DLSCT requires no predetermined scanning and allows for retrospective spectral analysis on "simultaneous and homologous" imaging in a routine scan, which is worth promoting.

Conclusions

The quantitative DECT spectral parameters showed potential in predicting VEDM in CRC following surgery in this preliminary study, which were in close relation with spectral perfusion in the venous phase. These spectral parameters are likely to help improve the efficiency of traditional clinical predictors. However, further verification will be necessary through researches with larger samples in the future.

Acknowledgments

The authors thank Hongyu Zhang, Xuelian Ji, and technicians in the Department of Radiology for their assistance in collecting patients. Thanks also go to Editage (https://www.editage.cn) for its linguistic assistance during the preparation of the manuscript.

Funding: This work was supported by the CAMS Innovation Fund for Medical Sciences (CIFMS) (No. 2021-I2M-C&T-A-017 to H.Z.), the Capital's Funds for Health Improvement and Research (CFH) (No. 2022-2-4024 to H.Z.), the National Natural Science Foundation of China (No. 81971589 to H.Z.), the 2020 SKY Imaging Research Fund (No. Z-2014-07-2003-01 to H.Z.), and the CAMS Innovation Fund for Medical Sciences (CIFMS) (No. 2022-I2M-C&T-B-077 to H.Z.).

Footnote

Reporting Checklist: The authors have completed the TRIPOD reporting checklist. Available at https://qims.amegroups.com/article/view/10.21037/qims-23-861/rc

Conflicts of Interest: All authors have completed the ICMJE uniform disclosure form (available at https://qims.amegroups.com/article/view/10.21037/qims-23-861/coif). S.D. reports serving as a full-time employee of Philips Healthcare during the conduct of the study. H.Z. was supported by grants from the CAMS Innovation Fund for Medical Sciences (CIFMS) (No. 2021-I2M-C&T-A-017), grants from the Capital's Funds for Health Improvement and Research (CFH) (No. 2022-2-4024), grants from the National Natural Science Foundation of China (No. 81971589), grants from the 2020 SKY Imaging Research Fund (No. Z-2014-07-2003-01), and grants from the CAMS Innovation Fund for Medical Sciences (CIFMS) (No. 2022-I2M-C&T-B-077). The other authors have no conflicts of interest to declare.

Ethical Statement: The authors are accountable for all aspects of the work in ensuring that questions related to the accuracy or integrity of any part of the work are appropriately investigated and resolved. This study was conducted in accordance with the Declaration of Helsinki (as revised in 2013). The study protocol was approved by the Institutional Review Board of Chinese Academy of Medical Sciences and Peking Union Medical College (No. 2021-I2M-C&T-A-017), and written informed consent was provided by each patient before the CT examination.

References

1. Benson AB, Venook AP, Al-Hawary MM, Arain MA, Chen YJ, Ciombor KK, et al. NCCN Guidelines Insights: Rectal Cancer, Version 6.2020. J Natl Compr Canc Netw 2020;18:806-15.
2. Benson AB, Venook AP, Al-Hawary MM, Arain MA, Chen YJ, Ciombor KK, et al. Colon Cancer, Version 2.2021, NCCN Clinical Practice Guidelines in Oncology. J Natl Compr Canc Netw 2021;19:329-59.
3. Wakai T, Shirai Y, Sakata J, Kameyama H, Nogami H, Iiai T, Ajioka Y, Hatakeyama K. Histologic evaluation of intrahepatic micrometastases in patients treated with or without neoadjuvant chemotherapy for colorectal carcinoma liver metastasis. Int J Clin Exp Pathol 2012;5:308-14.
4. Benoist S, Nordlinger B. The role of preoperative chemotherapy in patients with resectable colorectal liver metastases. Ann Surg Oncol 2009;16:2385-90.
5. D'Souza N, Shaw A, Lord A, Balyasnikova S, Abulafi M, Tekkis P, Brown G. Assessment of a Staging System for Sigmoid Colon Cancer Based on Tumor Deposits and Extramural Venous Invasion on Computed Tomography. JAMA Netw Open 2019;2:e1916987.
6. Kim TH, Woo S, Han S, Suh CH, Vargas HA. The Diagnostic Performance of MRI for Detection of Extramural Venous Invasion in Colorectal Cancer: A Systematic Review and Meta-Analysis of the Literature. AJR Am J Roentgenol 2019;213:575-85.
7. Bae JS, Kim SH, Hur BY, Chang W, Park J, Park HE, Kim JH, Kang HJ, Yu MH, Han JK. Prognostic value of MRI in assessing extramural venous invasion in rectal cancer: multi-readers' diagnostic performance. Eur Radiol 2019;29:4379-88.
8. Liemburg GB, Brandenbarg D, Berger MY, Duijts SFA, Holtman GA, de Bock GH, Korevaar JC, Berendsen AJ. Diagnostic accuracy of follow-up tests for detecting colorectal cancer recurrences in primary care: A systematic review and meta-analysis. Eur J Cancer Care (Engl) 2021;30:e13432.
9. Ritts RE Jr, Del Villano BC, Go VL, Herberman RB, Klug TL, Zurawski VR Jr. Initial clinical evaluation of an immunoradiometric assay for CA 19-9 using the NCI serum bank. Int J Cancer 1984;33:339-45.
10. Al-Najami I, Mahmoud Sheta H, Baatrup G. Differentiation between malignant and benign rectal tumors by dual-energy computed tomography - a feasibility study. Acta Oncol 2019;58:S55-9.
11. Al-Najami I, Beets-Tan RG, Madsen G, Baatrup G. Dual-Energy CT of Rectal Cancer Specimens: A CT-based Method for Mesorectal Lymph Node Characterization. Dis Colon Rectum 2016;59:640-7.
12. Wu J, Lv Y, Wang N, Zhao Y, Zhang P, Liu Y, Chen A, Li J, Li X, Guo Y, Wu T, Liu A. The value of single-source dual-energy CT imaging for discriminating microsatellite instability from microsatellite stability human colorectal cancer. Eur Radiol 2019;29:3782-90.
13. Mulé S, Pigneur F, Quelever R, Tenenhaus A, Baranes L, Richard P, Tacher V, Herin E, Pasquier H, Ronot M, Rahmouni A, Vilgrain V, Luciani A. Can dual-energy CT replace perfusion CT for the functional evaluation of advanced hepatocellular carcinoma? Eur Radiol 2018;28:1977-85.
14. Stiller W, Skornitzke S, Fritz F, Klauss M, Hansen J, Pahn G, Grenacher L, Kauczor HU. Correlation of quantitative dual-energy computed tomography iodine maps and abdominal computed tomography perfusion measurements: are single-acquisition dual-energy computed tomography iodine maps more than a reduced-dose surrogate of conventional computed tomography perfusion? Invest Radiol 2015;50:703-8.
15. Kang HJ, Kim SH, Bae JS, Jeon SK, Han JK. Can quantitative iodine parameters on DECT replace perfusion CT parameters in colorectal cancers? Eur Radiol 2018;28:4775-82.
16. Qiu L, Hu J, Weng Z, Liu S, Jiang G, Cai X. A prospective study of dual-energy computed tomography for differentiating metastatic and non-metastatic lymph nodes of colorectal cancer. Quant Imaging Med Surg 2021;11:3448-59.
17. Rada M, Lazaris A, Kapelanski-Lamoureux A, Mayer TZ, Metrakos P. Tumor microenvironment conditions that favor vessel co-option in colorectal cancer liver metastases: A theoretical model. Semin Cancer Biol 2021;71:52-64.
18. Kim KW, Lee JM, Klotz E, Park HS, Lee DH, Kim JY, Kim SJ, Kim SH, Lee JY, Han JK, Choi BI. Quantitative

CT color mapping of the arterial enhancement fraction of the liver to detect hepatocellular carcinoma. Radiology 2009;250:425-34.
19. Baxa J, Vondráková A, Matoušková T, Růžičková O, Schmidt B, Flohr T, Sedlmair M, Ferda J. Dual-phase dual-energy CT in patients with lung cancer: assessment of the additional value of iodine quantification in lymph node therapy response. Eur Radiol 2014;24:1981-8.
20. Hunter C, Siddiqui M, Georgiou Delisle T, Blake H, Jeyadevan N, Abulafi M, Swift I, Toomey P, Brown G. CT and 3-T MRI accurately identify T3c disease in colon cancer, which strongly predicts disease-free survival. Clin Radiol 2017;72:307-15.
21. Beets-Tan RGH, Lambregts DMJ, Maas M, Bipat S, Barbaro B, Curvo-Semedo L, Fenlon HM, Gollub MJ, Gourtsoyianni S, Halligan S, Hoeffel C, Kim SH, Laghi A, Maier A, Rafaelsen SR, Stoker J, Taylor SA, Torkzad MR, Blomqvist L. Magnetic resonance imaging for clinical management of rectal cancer: Updated recommendations from the 2016 European Society of Gastrointestinal and Abdominal Radiology (ESGAR) consensus meeting. Eur Radiol 2018;28:1465-75.
22. Peinado H, Zhang H, Matei IR, Costa-Silva B, Hoshino A, Rodrigues G, Psaila B, Kaplan RN, Bromberg JF, Kang Y, Bissell MJ, Cox TR, Giaccia AJ, Erler JT, Hiratsuka S, Ghajar CM, Lyden D. Pre-metastatic niches: organ-specific homes for metastases. Nat Rev Cancer 2017;17:302-17.
23. Lagarde SM, Phillips AW, Navidi M, Disep B, Immanuel A, Griffin SM. The presence of lymphovascular and perineural infiltration after neoadjuvant therapy and oesophagectomy identifies patients at high risk for recurrence. Br J Cancer 2015;113:1427-33.
24. Wang Z, Tang Y, Tan Y, Wei Q, Yu W. Cancer-associated fibroblasts in radiotherapy: challenges and new opportunities. Cell Commun Signal 2019;17:47.
25. Ulyte A, Katsaros VK, Liouta E, Stranjalis G, Boskos C, Papanikolaou N, Usinskiene J, Bisdas S. Prognostic value of preoperative dynamic contrast-enhanced MRI perfusion parameters for high-grade glioma patients. Neuroradiology 2016;58:1197-208.
26. Li Q, Li X, Li XY, Huo JW, Lv FJ, Luo TY. Spectral CT in Lung Cancer: Usefulness of Iodine Concentration for Evaluation of Tumor Angiogenesis and Prognosis. AJR Am J Roentgenol 2020;215:595-602.
27. Gao L, Lu X, Wen Q, Hou Y. Added value of spectral parameters for the assessment of lymph node metastasis of lung cancer with dual-layer spectral detector computed tomography. Quant Imaging Med Surg 2021;11:2622-33.
28. Wang YL, Zhang HW, Mo YQ, Zhong H, Liu WM, Lei Y, Lin F. Application of dual-layer spectral detector computed tomography to evaluate the expression of Ki-67 in colorectal cancer. J Chin Med Assoc 2022;85:610-6.
29. Li R, Li J, Wang X, Liang P, Gao J. Detection of gastric cancer and its histological type based on iodine concentration in spectral CT. Cancer Imaging 2018;18:42.
30. Gao W, Zhang Y, Dou Y, Zhao L, Wu H, Yang Z, Liu A, Zhu L, Hao F. Association between extramural vascular invasion and iodine quantification using dual-energy computed tomography of rectal cancer: a preliminary study. Eur J Radiol 2023;158:110618.
31. Li J, Xu S, Wang Y, Fang M, Ma F, Xu C, Li H. Spectral CT-based nomogram for preoperative prediction of perineural invasion in locally advanced gastric cancer: a prospective study. Eur Radiol 2023;33:5172-83.
32. Aoki M, Takai Y, Narita Y, Hirose K, Sato M, Akimoto H, Kawaguchi H, Hatayama Y, Miura H, Ono S. Correlation between tumor size and blood volume in lung tumors: a prospective study on dual-energy gemstone spectral CT imaging. J Radiat Res 2014;55:917-23.

Cite this article as: Peng W, Wan L, Zhao R, Chen S, Dong S, Li L, Zhang H. Novel biomarkers based on dual-energy computed tomography for risk stratification of very early distant metastasis in colorectal cancer after surgery. Quant Imaging Med Surg 2024;14(1):618-632. doi: 10.21037/qims-23-861